



Soft Matter

**Kinetically-Arrested Single-Polymer Nanostructures from
Amphiphilic Mikto-Grafted Bottlebrushes in Solution: A
Simulation Study**

Journal:	<i>Soft Matter</i>
Manuscript ID	SM-ART-04-2020-000771
Article Type:	Paper
Date Submitted by the Author:	29-Apr-2020
Complete List of Authors:	Gumus, Bahar; University of Texas at San Antonio, Chemical Engineering Herrera-Alonso, Margarita; Colorado State University, Chemical and Biological Engineering Ramirez-Hernandez, Abelardo; University of Texas at San Antonio, Chemical Engineering

SCHOLARONE™
Manuscripts

ARTICLE

Kinetically-Arrested Single-Polymer Nanostructures from Amphiphilic Mikto-Grafted Bottlebrushes in Solution: A Simulation Study

Received 00th January 20xx,
Accepted 00th January 20xx

DOI: 10.1039/x0xx00000x

Bahar Gumus,^a Margarita Herrera-Alonso^c and Abelardo Ramírez-Hernández^{* a,b}

Solution self-assembly of molecular bottlebrushes offers a rich platform to create complex functional organic nanostructures. Recently, it has become evident that kinetics, not just thermodynamics, plays an important role in defining the self-assembled structures that can be formed. In this work, we present results from extensive molecular dynamics simulations that explore the self-assembly behavior of mikto-grafted bottlebrushes when the solvent quality for one of the side blocks is changed by a rapid quench. We have performed a systematic study of the effect of different structural parameters and the degree of incompatibility between side chains on the final self-assembled nanostructures in the low concentration limit. We found that kinetically-trapped complex nanostructures are prevalent as the number of macromonomers increases. We performed a quantitative analysis of the self-assembled morphologies by computing the radius of gyration tensor and relative shape anisotropy as the different relevant parameters were varied. Our results are summarized in terms of non-equilibrium morphology diagrams.

Introduction

Block copolymers are a versatile class of macromolecular materials which can spontaneously self-assemble into a myriad of different nanostructures both in solution conditions as well as in the melt state¹⁻³. Precise control of the size and morphology of these nanostructures is achieved by manipulating both molecular and process parameters³⁻⁵. In particular, polymer architecture, degree of polymerization and composition are three key structural parameters that can be used to design organic nanostructures from the bottom-up^{3, 6, 7}. In the case of linear block polymers, by playing with composition, degree of polymerization and blocks' sequence, a plethora of different structures can be realized^{8, 9}. The other dimension in this parameter space, corresponding to polymer architecture, has been started to be explored in a more systematic way¹⁰⁻¹², however a fundamental understanding of the principles governing the self-assembly has not been achieved yet, as in the case of linear diblock polymers. A particularly important class of macromolecules with elaborated architecture are the so-called molecular bottlebrushes, these are graft polymers where the distance between grafting points along the backbone is smaller than the characteristic dimensions of the grafted-chains¹³⁻¹⁸. This

structural feature endows these materials with three characteristic properties: *i*) a high concentration of side-chains, *ii*) extended conformations, and *iii*) a dramatic increase in the molecular weight of entanglement¹⁵. These features cause bottlebrushes to display distinctive behaviors not present in simple linear polymers. More importantly, those three emergent properties arise from the macromolecular architecture alone rather than from any specific chemistry. Thus, given the immense palette of possible chemical components that could be used to synthesize bottlebrushes, it is expected that novel functionalities can become feasible that are difficult or impossible to achieve with simple linear polymers^{14, 16, 17}. Bottlebrush polymers are synthesized mainly by three polymerization techniques¹⁷: (1) grafting- from (polymerization of monomers from the backbone), (2) grafting-to (attachment of side chains to the backbone), and (3) grafting-through (polymerization of macromonomers). By using these polymerization tools, it is possible to create molecular bottlebrushes with many structural variations: branched, brush-coil, linear, among others^{15, 17}. It is common to use a combination of these methodologies to synthesize multicomponent bottlebrushes, such as mikto-grafted and core-shell bottlebrushes. These multicomponent bottlebrushes can then be used to generate well-defined nanostructured objects by solution self-assembly, or to fabricate periodic nanostructured materials with large domain spacings by self-assembly in melt conditions^{15, 19, 20}.

Solution self-assembly of block polymers is an important methodology to create functional organic nanoparticles^{2, 21, 22}. Solution self-assembly of molecular bottlebrushes thus offer a rich platform to create advanced materials with potential applications such as well-defined metal-organic nano-objects, stimuli-responsive aggregates, photonic materials, drug delivery systems, and porous nanoparticles^{15, 17, 23-26}. However, even in the simple case of linear

^a Department of Biomedical Engineering and Chemical Engineering, The University of Texas San Antonio, TX 78249, United States.
email: abelardo.ramirez-hernandez@utsa.edu

^b Department of Physics and Astronomy, The University of Texas at San Antonio, San Antonio, Texas 78249, United States

^c Chemical & Biological Engineering & School of Advanced Materials Discovery, Colorado State University, Fort Collins, Colorado 80523, United States.

*Electronic Supplementary Information (ESI) available: Additional results regarding the stability and diversity of the nanostructures are provided. See DOI: 10.1039/x0xx00000x

block polymers, the prediction of possible polymer aggregates in solution is a challenge, not only because of the complexity of the systems, but also because non-ergodic behavior can arise under certain solvent conditions²⁷⁻³². Thus, non-equilibrium polymer aggregates are possible, and probably the rule rather than the exception, in most of the experimental situations. In fact, in the case of mikto-grafted bottlebrushes, it has been shown that kinetically-arrested polymer nanostructures can be created by the combined effect of solvent quality changes and shear forces that arise during the mixing of the solution^{30, 33}. Nevertheless, a fundamental understanding of equilibrium and non-equilibrium self-assembly of bottlebrushes, and the implications of their structural parameters on it, is still lacking.

Computer simulations are a powerful tool with the potential of providing physical insights about the relevant microscopic parameters involved in the self-organization of bottlebrushes^{34, 35}. The first computational study on bottlebrushes focused on the structural features of single-molecule homogeneous and two-component molecular bottlebrushes modeled on a lattice under both, good and bad solvent conditions³⁶⁻³⁸. Yethiraj performed gridless Monte Carlo simulations of a single-bottlebrush homopolymer by representing each bead as a hard sphere³⁹. He explored the statistical conformational properties as a function of backbone molecular weight and side chain's length. In more recent works, Lennard-Jones models have been used to explore the behavior of bottlebrushes in solutions, melts and networks⁴⁰⁻⁵². An interesting approach was put forward by Lyubimov et al. where they proposed a hybrid approach by combining molecular dynamics simulation and the Polymer Reference Interaction Site Model (PRISM) theory to study of self-assembly of amphiphilic bottlebrush polymers^{53, 54}. All these studies have provided valuable information regarding the statistical properties of the model bottlebrushes studied in those works. However, given the computational costs to represent these large macromolecules, all the studies focused on multi-bottlebrush simulations using Lennard-Jones models have been restricted to study relatively small molecules (3-5 beads per side chain and a small number of macromonomers). Thus, by using such microscopic approaches it becomes complicated to explore the organization of bottlebrushes with a large number of macromonomers, that in turn, also contain side chains with a large polymerization index. For this reason, in this work we use a coarser approach to represent molecular bottlebrushes, where intermolecular interactions are softer, such approach has been successfully used to explore the large-scale organization of lipid membranes, and thus, we expect that this simulation framework would be able to correctly capture the physics of bottlebrushes at this mesoscopic level of description.

We are particularly interested in the phenomenology reported in a series of experiments regarding the solution self-assembly of *poly(glycidyl methacrylate)-g-poly(ethylene glycol)/poly(lactic acid)* [PGMA-g-PEG/PLA] bottlebrushes^{30, 33, 55}, this double-brush architecture consist of side-chains of poly(D,L-lactide) [PLA] and poly(ethylene glycol) [PEG]. It was shown that by manipulating the ratio of hydrophilic (PEG) to hydrophobic (PLA) side chains and the global molecular weight, these bottlebrushes could self-assemble into spherical and cylindrical micelles, as well as vesicles, in the

presence of selective solvents. Interestingly, toroidal micelles were also found to be formed under certain conditions³³. However, it is not clear if all of these polymer aggregates formed as equilibrium structures or if the flow field in combination with solvent quality changes induced their formation and stability, and therefore they are non-equilibrium nanostructures. It was also found that most of the polymer nanostructures were formed by single molecules⁵⁶, thus offering an intriguing case to be explored by molecular simulations. The very low aggregation numbers of these macromolecular aggregates can be explained by the fact that for every solvophobic side chain, there is one solvophilic side chain, thus the areal density of solvophilic chains is high enough to act like a brush that stabilizes solvophobic cores against fusion. It should also be highlighted that recent experimental work has found that solutes can induce morphological transitions of the self-assembled structures of these bottlebrushes^{57, 58}. However, little is known about the behavior of these materials in the presence of added solutes. In this work, we use a coarse-grained molecular model to explore the self-assembly of single amphiphilic mikto-grafted bottlebrushes in solution. Our simulations are focused on the self-assembly of bottlebrushes in response to a fast quench in solvent selectivity for one of the side blocks. We have performed an extensive and systematic study of the effect of different structural parameters and the degree of incompatibility between side chains on the final self-assembled nanostructures. We have found that kinetically-trapped complex nanostructures are more common as the number of macromonomers increases, and when the incompatibility between side chains is large. We summarize our simulation results in terms of non-equilibrium morphology diagrams.

Model and Methods

As mentioned in the Introduction, in this report we aimed to explore the large time and length scales, much larger than those achieved with ordinary molecular dynamics simulations based on an atomistic description, associated to the complex molecular systems of interest. Thus, we use a coarse-grained approach to model amphiphilic mikto-grafted bottlebrushes. This coarse-grained approach contains information regarding the molecular architecture of the macromolecules, and the chemical details are encoded into generic intermolecular interaction parameters⁵⁹. Polymers are represented

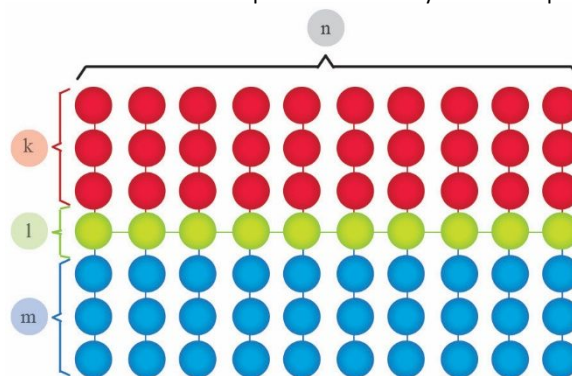


Figure 1. Schematic representation of the mikto-grafted bottlebrush architecture considered in this work ($C-g-A_k/B_m$)_n. Solvophobic molecular units are represented by A beads (red), whereas B beads (blue) are solvophilic. Backbone molecular units (C, green beads) are slightly solvophobic.

by a bead-spring model, with each bottlebrush composed by n identical macromonomers, and each macromonomer is a linear triblock oligomer $A_k C_l B_m$, where the subindices represent the number of beads that each block is composed of. In this work we fixed $l = 1$, and each C bead on a given macromonomer is connected to another C bead on another macromonomer, thus forming the bottlebrush backbone. Our mikto-grafted bottlebrush molecule is then denoted by $(C-g-A_k/B_m)_n$ (see Figure 1 for details). It should be noted here that a very similar molecular structure has been studied in melt state with the use of Self-Consistent Mean Field Theory^{60, 61}. We consider two architecturally different structures: symmetric ($k = m$) and asymmetric ($k \neq m$) side chains. In our modeling, beads type A represent solvophobic molecular units, and B beads represent solvophilic entities. The backbone units (C beads) are assumed to be slightly solvophobic. The solvent is explicitly incorporated into the simulations and it is represented by beads of type D. Intra-molecular k_2 interactions between two bonded beads are given by $u_{intra} = \frac{1}{2} (\mathbf{r}_{ij} - \ell_0)^2$, where the distance between two particles is \mathbf{r}_{ij} , the equilibrium bond length is ℓ_0 , and the bond coupling constant is denoted by k_2 .

We use the Dissipative Particle Dynamics (DPD)⁶²⁻⁶⁴ technique to explore the mesoscale dynamics of the molecular systems of interest in this work. The inter-molecular interactions are represented by soft potentials which allow for the large time and length scales to be simulated. Explicitly, the effective intermolecular force that a bead i feels due to the interaction with a bead j , is given by $\vec{F}_{ij} = \vec{F}_{ij}^C + \vec{F}_{ij}^D + \vec{F}_{ij}^R$. This force has conservative, dissipative and random pairwise contributions, all of these are central forces and the corresponding magnitudes are: $F_{ij}^C = a_{ij}(1 - r_{ij}/r_0)$, $F_{ij}^D = -\gamma(1 - r_{ij}/r_0)(\hat{r}_{ij} \cdot \vec{v}_{ij})$ and $F_{ij}^R = \sigma(1 - r_{ij}/r_0)\xi_{ij}$, for $r_{ij} \leq r_0$ and are zero otherwise. $\vec{v}_{ij} = \vec{v}_i - \vec{v}_j$ is the relative velocity between the two interacting particles, γ and σ represent the strength of dissipation and fluctuation, respectively. To ensure the local momentum conservation, the random force has the symmetry property $\xi_{ij} = \xi_{ji}$, also γ and σ are related via the fluctuation-dissipation theorem⁶⁵, $\sigma^2 = 2\gamma k_B T$, where the Boltzmann constant and temperature are k_B and T , respectively. Note that r_0 can be interpreted as the diameter of soft spheres representing the beads. Thus, all beads, including solvent beads, are assumed to have the same size. We use r_0 and $k_B T$ as length and energy units, respectively. The parameters a_{ij} quantify the repulsion between beads, representing the exclude volume interactions and the chemical incompatibility between unlike monomers.

Following previous works addressing the self-assembly of polymersomes⁶⁶⁻⁶⁸ and the fusion of lipid membranes⁶⁹⁻⁷¹, the interaction parameters were chosen as follows: $k_2 = 128 k_B T / r_0^2$, $\ell_0 = 0.75 r_0$, $\sigma = 3$, and the reduce number density is fixed to $\rho = 3$. Following Groot and Warren⁷², the self-interactions are fixed to $a_{AA} = a_{BB} = a_{CC} = a_{DD} = 25 k_B T / r_0$, which comes from the requirement that a pure fluid of each bead type possesses the same compressibility of water⁵. To select the rest of intermolecular interaction parameters we considered the relationship between the Flory-Huggins parameter, χ_{ij} , and the strength of the soft repulsions, a_{ij} , that was established in Ref. [72], namely: $a_{ij} \approx a_{ii} + 3.497 \chi_{ij}$ (for $\rho = 3$). By using this expression for a polymer immersed in a theta solvent ($\chi_{pol-solv} = 0.5$), then the corresponding DPD

interaction parameter should have the value $a_{pol-solv} \approx 27$. Thus, values lower than 27 represent good solvent conditions, whereas values larger than that number will correspond to a bad solvent. The particular case of $a_{pol-solv} = 25$, represents an athermal solvent. In this work we use $a_{BD} = 27$, thus polymer side chains composed by type B beads are in a solution very close to theta conditions. On the other hand, C beads are slightly solvophobic, thus, we set $a_{CD} = 30$. We also assume that the chemistry between A and C beads is similar, such that the chemical incompatibility is negligible, *i. e.* $a_{AC} = 25$. However, B and C are dissimilar and therefore we set $a_{BC} = 28$. To represent the highly solvophobic polymer side chains composed by A beads, we have chosen $a_{AD} = 70$. Finally, we have one interaction parameter to be investigated, a_{AB} , in addition to the bottlebrush's architectural parameters (k, m, n). To summarize, the intermolecular interaction parameters are shown in the following symmetric matrix:

$$\begin{bmatrix} & A & B & C & D \\ A & 25 & a_{AB} & 25 & 70 \\ B & a_{AB} & 25 & 28 & 27 \\ C & 25 & 28 & 25 & 30 \\ D & 70 & 27 & 30 & 25 \end{bmatrix}$$

All simulations were performed using HOOMD-Blue⁷³⁻⁷⁵. The time step used to integrate the equations of motion is $\delta t = 0.01 \tau$, where $\tau = \sqrt{r_0^2 m / k_B T}$ and $m = 1$ is the mass of a DPD bead. Images were created using VMD⁷⁶. Our simulations take place within a box of constant volume $V = L_x L_y L_z$, and periodic boundary conditions are used in all directions. The simulation box is filled with DPD beads to the chosen density, ρ . In this work we are interested in nanostructures formed by single bottlebrushes in solution, thus, once the macromolecule's architectural parameters (k, m, n) are selected, the bottlebrush is created with a random configuration within the simulation box, then the box is filled with solvent beads (type D) by assigning random coordinates to them. The simulation box size is chosen to be big enough to avoid the self-interaction of the bottlebrush with its periodic image. The total number of beads (polymer and solvent beads) depended on the values of (k, m, n), and ranged from 10^5 to 3×10^6 beads. Simulations were performed by using the following protocol: First, initial configurations were relaxed with all intermolecular interactions $a_{ij} = 25$ ($\forall i, j$), thus, the solvent is an athermal solvent for all polymer blocks and there is not segregation between chemically dissimilar polymer segments. This step is performed for 10^5 time steps, after which macromolecules adopt a relaxed configuration. In the second step, a deep quench to a bad solvent condition, for the polymer segments of type A, is mimicked by an instantaneous change in the intermolecular interactions to those values on the matrix in Eq. 1. The production run for the second step is 5×10^5 to 1.5×10^6 time steps, depending on the bottlebrush's degree of polymerization. For each instance of the bottlebrush's architectural parameters (k, m, n) and intermolecular interactions explored, ten different initial random configurations were generated and evolved to gather statistics about the different polymer nanostructures that were obtained by the described protocol.

To characterize the polymer nanostructure size, shape and anisotropy we have computed the gyration tensor⁷⁷ $G_{\alpha\beta} = \frac{1}{M} \sum_k (r_k^\alpha - R_{com}^\alpha)(r_k^\beta - R_{com}^\beta)$, where the sum runs over all polymer

beads in the molecular bottlebrush, \mathbf{r}_k^α is the spatial coordinate α of the polymer bead k , and \mathbf{R}_{com}^α is the coordinate α associated to the center of mass of the bottlebrush. From the diagonalization of \mathbf{G} , other properties can be deduced⁷⁸⁻⁸⁰, as for example, the radius of gyration, $R_g^2 \equiv \lambda_1 + \lambda_2 + \lambda_3$, where λ_i 's are the eigenvalues of \mathbf{G} ($\lambda_1 \geq \lambda_2 \geq \lambda_3$), the relative shape anisotropy, $A_3 \equiv 3/2(\text{Tr } \mathbf{G}^2)/(\text{Tr } \mathbf{G})^2$, and asphericity, $b \equiv \lambda_1 - \frac{1}{2}(\lambda_2 + \lambda_3)$.

Results and Discussion

As mentioned above, in this work, we focus on the solution self-assembly of single-bottlebrushes. This section starts by presenting the simulation results obtained for symmetric ($\mathbf{k} = \mathbf{m}$) molecular bottlebrushes (C-g-A_k/B_m)_n. For these calculations, the number of macromonomers, \mathbf{n} , was varied from $\mathbf{n} = 100$ to $\mathbf{n} = 1000$, and the side chains' degree of polymerization was varied from $\mathbf{k} = 10$ to $\mathbf{k} = 50$. The effect of the chemical incompatibility between A and B side chains on the self-assembled morphology was also studied, two different values were considered: $\mathbf{a}_{AB} = 30$ (weak incompatibility) and $\mathbf{a}_{AB} = 70$ (strong incompatibility). Based on the relationship, reported by Groot et al (Ref. 72), between DPD and Flory-Huggins parameters, these values should correspond to $\chi_{AB} \sim 1.4$ and $\chi_{AB} \sim 13$, thus being an order of magnitude different to each other. Our motivation was to explore the effect of this parameter in these two different regimes. As mentioned above, for each different instance of the architectural parameters ($\mathbf{k}, \mathbf{m}, \mathbf{n}$), ten different initial configurations were evolved following the simulation protocol described in the Methods section. We found that for a large enough number of macromonomers, different initial configurations could evolve into different self-assembled nanostructures (typically two or three different morphologies), particularly for the large AB incompatibility. In **Figure 2**, we display those self-assembled nanostructures that appeared more frequently in symmetric molecular bottlebrushes for both incompatibility values, \mathbf{a}_{AB} , used in our calculations. To build the morphology diagrams presented in **Figure 3a** and **4a**, we selected those morphologies that appeared more frequently among the ten different initial configurations for each point in the explored parameter space.

Our simulation results for $\mathbf{a}_{AB} = 30$ are summarized in the morphology diagram on the parameter space (\mathbf{n}, \mathbf{k}) presented in **Figure 3a**. As can be seen, when the number of macromonomers, \mathbf{n} , is small (less than 400), spherical micelles are always formed for any degree of polymerization of the side chains. For these architectural features, the bottlebrush backbone folds around the spheres formed by the solvophobic, type A, polymer segments (see **Figure 2**). This collapse has to be such that there is not an area of the solvophobic core exposed to the solvent. Note that the flexibility of the chains has a strong influence on the way the folding happens on the surface of the solvophobic core. In our model, polymer chains are fully flexible, therefore hairpin-like conformations are not strongly penalized and can occur with high frequency if that would help to minimize the contact between type A polymer segments and the solvent. This situation will change if semiflexible backbones were used instead⁸¹.

Note that the motion of the backbone is strongly correlated to the motion of side chains. Thus, it is expected that the collapse dynamics of the bottlebrush backbone will be strongly dependent on the

dynamic features of the side chains. For example, if side chain dynamics is slow, as in the case when they are below their glass transition temperature, or if they are long enough to be entangled, the backbone collapse will also be slow even though its own dynamical features are not that of a chain below its glass transition temperature. Thus, the collapse is not unique, but it can depend on the pathway that the bottlebrush followed; if the solvophobic core has fluid-like properties, then the folded backbone will sample different conformations.

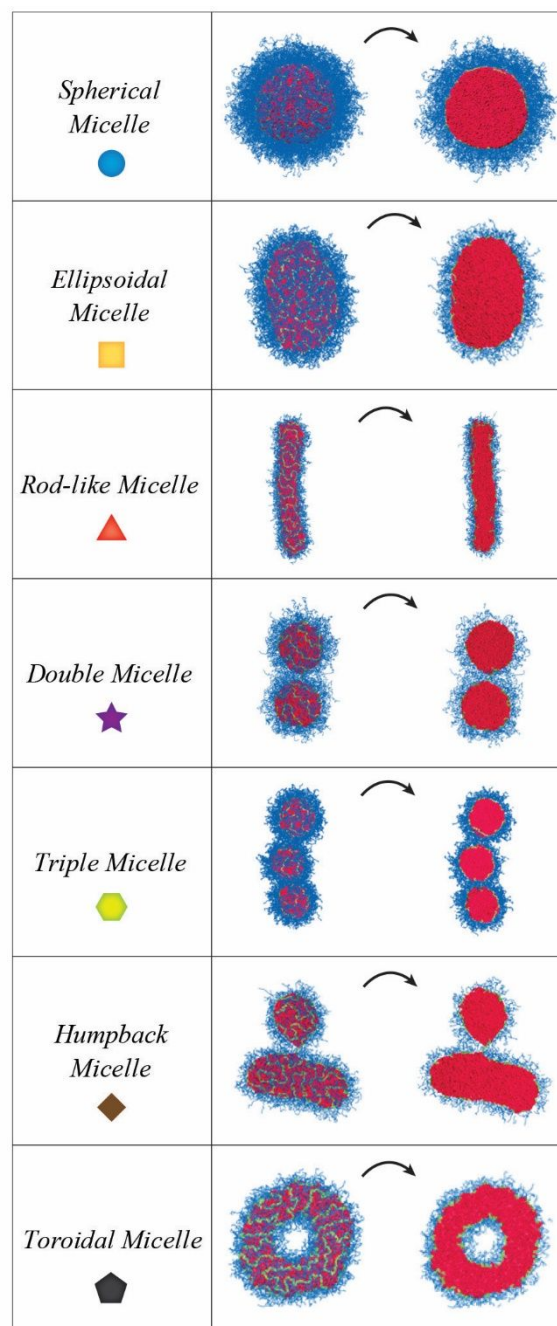


Figure 2. Representative single-polymer self-assembled nanostructures obtained after a fast quench into a bad solvent condition for one of the side chains (red domains). Solvophilic side chains are displayed in blue, whereas the bottlebrush backbone is represented by the green tube wrapping around the solvophobic cores. Solvent molecules are not displayed for clarity. Two snapshots are presented, the image on the right is a cross-section of the image on the left. We also indicate the symbols used in the morphology diagrams presented in **Figures 3a** and **4a**. Images are not at the same scale.

By increasing the number of macromonomers to $n = 400$, a morphological transition occurs when side chain's degree of polymerization is small ($k < 20$). Instead of a spherical micelle, the bottlebrush now self-assembled into an ellipsoidal micelle (see **Figure 2**). As in the case of spherical micelles, the solvophobic polymer segments form a core, but with an ellipsoidal shape, and the backbone also wraps around it in a complicated folded conformation. In turn, the solvophilic segments form a corona that interacts with solvent molecules, screening the dissimilar interactions between the type A segments and the solvent. If the side chains' degree of polymerization is larger than 20, then, the nanostructures that are formed after bottlebrush collapse are spherical micelles once again (see morphology diagram in **Figure 3a**). By increasing the bottlebrush backbone molecular weight to values $500 < n < 1000$, then a scenario with three different morphologies takes place. For large enough side chains, spherical micelles are always formed, but for degrees of polymerization below a critical value, $k_c(n)$, that depends on the number of macromonomers, a morphological transition to ellipsoidal micelles occurs. There is, however, a second transition that takes place at smaller degrees of polymerization, $k_r(n)$, below which the bottlebrushes collapse into rod-like micelles (see **Figures 2** and **3a**). These elongated nanostructures have a cross-sectional area (perpendicular to the long axis) that is independent of the number of macromonomers for constant side chain's molecular weight. However, as can be seen in the color map of the radius of gyration of the nanostructures (**Figure 3b**), the length of the rod is controlled by n , thus, providing a recipe to create organic rods of specific sizes. Also note that the density map of the relative shape

anisotropy (**Figure 3c**) correctly captures the expected large anisotropy of these nanorods. The relative shape anisotropy is zero for a completely symmetrical object (spherical micelle), it reaches a value of 1/4 for a very thin circular disk-like object and becomes 1 for a rod with an infinitesimal width. As can be seen in the density color maps, the rod-like micelles' shape anisotropy reaches a value ~ 0.6 when the side chains are short, and decreases in value as the side chain molecular weight increases. Note also that ellipsoidal micelles possess relative shape anisotropies in the range $0.15 \leq A_3 \leq 0.35$. Note that relative shape anisotropy density map mirrors the whole morphology diagram, and it could, by itself, be a good order parameter to explore morphology diagrams in a more quantitative way. One interesting result is that the largest bottlebrushes studied in this work, $n = 1000$, self-assembled into toroidal micelles when the side chains are short (see **Figures 2** and **3a**). As mentioned above, for large n and small k , it is common that bottlebrushes self-assemble into more than two different morphologies. In the case of these toroidal micelles, they appeared 4/10 and 8/10 times when side chains lengths were $k = 10$ and $k = 20$, respectively. Morphology diagrams that include the frequency that each of the reported morphologies appeared are presented in the Supplementary Information. Note that both the relative shape anisotropy (**Figure 3c**) and radius of gyration (**Figure 3b**) for these toroidal micelles decrease in value, as expected due to their symmetry and loop configuration.

It should be highlighted that toroidal condensates have been observed in semi-flexible, collapsed homopolymer chains in the presence of poor solvents, both in simulations⁸²⁻⁸⁵ and experiments⁸⁶. The stiffness of the chains makes a compact spherical condensate unfavorable, as this entails a large bending penalty. Thus, chains prefer to arrange themselves into toroidal condensates. In our simulations, even though the model does not include bending interactions between consecutive polymer beads, the bottlebrushes possess an effective stiffness that arise from the high grafting density of side chains. Also, by forming a toroidal structure, the excess free energy associated with having two end caps is eliminated. Interestingly, the dynamic simulations of Ref. ⁸² showed the existence of different long-live intermediate states, including the so-called "racquets", that appear before the semi-flexible chains eventually reached the toroidal morphologies. In our simulations we also observed the formation of similar structures, two of these configurations are presented in the Supplementary Information.

Simulation results for the higher incompatibility between A and B beads explored in this work, $a_{AB} = 70$, are summarized in the morphology diagram on the parameter space (n, k) presented in **Figure 4a**. As can be deduced by comparing this morphology map and that one of the $a_{AB} = 30$ case, the diversity of morphologies displayed by these molecular systems is larger, but also, the self-assembled nanostructures possess more complexity. The first important observation is that the region on the parameter space that gives place to spherical micelles is larger than in the previous case. This can be rationalized by the fact that by increasing the chemical incompatibility between A and B beads, the interfacial energy increases^{87, 88} ($\gamma_{AB} \sim \chi_{AB}^{1/2}$). Thus, the core composed by type A particles will tend to decrease the area of contact between A and B beads, which is accomplished by forming a sphere. For a given

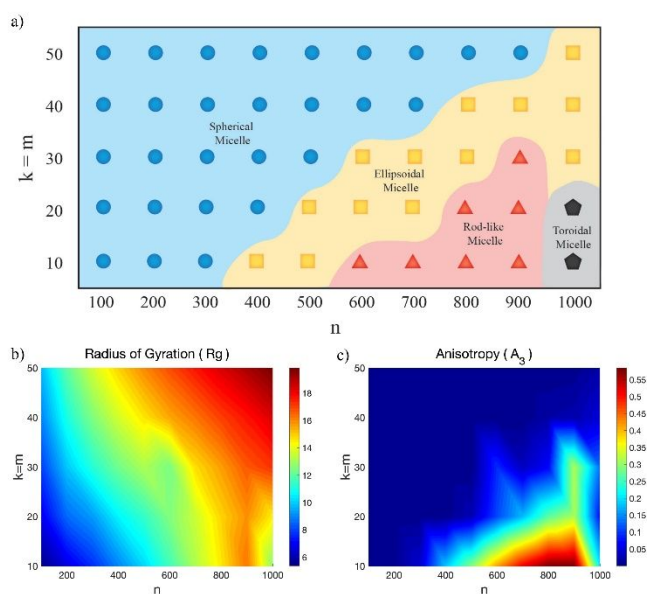


Figure 3. (a) Morphology diagram of symmetric ($k = m$) molecular bottlebrushes ($C_g A_n/B_m$)_n in the parameter space (n, k) representing the number of macromonomers and side chains' degree of polymerization, respectively, for weak incompatibility ($a_{AB} = 30$). Each morphology represents the more frequent structure (of ten different initial configurations) that is obtained following the simulation protocol described in the Methods section. (b) Color map of the radius of gyration, R_g , of the morphology at every point on the parameter space (n, k) . (c) Color map of the relative shape anisotropy, A_3 , of the morphology at every point on the parameter space (n, k) . The quantities displayed in (b) and (c) are the average property taken over the set of initial configurations that evolved to the same more frequent morphology.

number of A polymer segments, spherical cores have the optimal surface-to-volume ratio that minimizes the interfacial free energy cost. Ellipsoidal micelles still occur in the morphology diagram, but they appear at lower side-chain molecular weight.

Interestingly, when the number of macromonomers is $400 < n < 800$, a new morphology appears at intermediate side chain polymerization indices. Instead of self-assembling into rod-like micelles or ellipsoidal micelles, the bottlebrush forms two globes. This peculiar nanostructure is formed by the collapse of two sections of the bottlebrush, in an independent manner, into spherical micelles that are connected by the backbone. We hypothesize that these double micelles are kinetically-trapped morphologies that arise by the combination of a deep quench into a preferential solvent condition (selective for type B segments), and the strong incompatibility between A and B polymer segments. By having long bottlebrush backbones, the distant sections of the macromolecules do not have a collective response to the changes in the environment, but instead they respond locally to those changes. Thus, once the solvent conditions change rapidly to the selective solvent situation, the solvophobic segments start to collapse into local minimum free energy configurations, which decrease the dissimilar contacts between type A and solvent molecules as well as with type B polymer segments, that in this case are spherical micelles. These connected micelles are surrounded by a corona of type B segments, thus, the bottlebrush backbone connecting the two globes is also immersed within the corona, and it is not in contact with the solvent (see **Figure 2**).

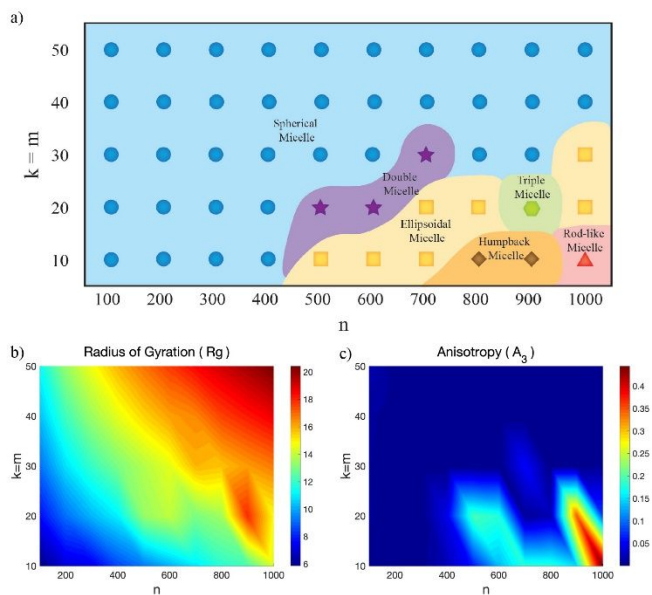


Figure 4. (a) Morphology diagram of symmetric ($k = m$) molecular bottlebrushes ($C_{4k}/B_{m,n}$) in the parameter space (n, k) representing the number of macromonomers and side chains' degree of polymerization, respectively, for strong incompatibility ($a_{AB} = 70$). Each morphology represents the more frequent structure (of ten different initial configurations) that is obtained following the simulation protocol described in the Methods section. (b) Color map of the radius of gyration, R_g , of the morphology at every point on the parameter space (n, k). (c) Color map of the relative shape anisotropy, A_3 , of the morphology at every point on the parameter space (n, k). The quantities displayed in (b) and (c) are the average property taken over the set of initial configurations that evolved to the same more frequent morphology.

The double micelle nanostructure could potentially relax into its equilibrium structure by fusing the two solvophobic cores, but this will require that type A side chains cross the bridge formed by type B beads, and this single-chain motion has a free-energy barrier^{89,90}, the possibility of having type A chains crossing the B domain is proportional to $\sim e^{-\alpha X_{AB}}$, where α is a quantity proportional to the block A molecular weight⁹¹. Thus, the stronger the incompatibility, the more difficult for the solvophobic chains to form a single agglomerate, and more probable for them to stay in these kinetically-trapped configurations. This also explains why these structures are not observed in the lower incompatibility case. To support this claim, we have performed additional simulations that started with double and triple micelle structures, and evolve them for 2×10^6 time steps by quenching to $a_{AB} = 30$. For comparison, same initial configurations were run for the same number of time steps keeping $a_{AB} = 70$. For the lower incompatibility case, double and triple micelles evolved toward a single-micelle structure, whereas they remain the same structures by keeping $a_{AB} = 70$ (see Figures S7 and S8 in the SI). These results support our statement about the importance of the incompatibility between A and B side chains on the kinetically-trapped structure formation.

By the same rationale explaining the existence of double micelles, one could expect that larger backbones could give place to multi-micelles: small spherical micelles connected by the bottlebrush backbone. In fact, our simulations show that this is the case: at $n = 900$ and $k = 20$, the bottlebrush self-assembled into a triple-micelle (see **Figures 2** and **4a**). We should note here that a linear arrangement of the three small spherical micelles is the more frequent structure (**Figure 2**), however, we also observed the formation of triple micelles arranged into a V shape. These elongated triple micelle structures have larger shape anisotropy values than ellipsoidal or spherical micelles (see **Figure 4c**). At small side chains polymerization index, $k = 10$, these bottlebrushes form another interesting structure: it is composed by a small satellite spherical micelle attached to a short rod-like micelle (labelled as humpback micelle in **Figure 2**). The shape anisotropy associated to this complex micelle has a noticeable increased value compared to that of spherical and ellipsoidal micelles. Finally, for the largest bottlebrushes, $n = 1000$, with short side chains, $k = 10$, rod-like micelles are formed. As can be inferred from **Figures 3c** and **4c**, both shape descriptors (shape anisotropy and radius of gyration) correctly capture the morphological changes that these complex macromolecules undergo as its structural parameters are varied. Note in particular, the large shape anisotropy that rod-like micelles and triple-micelle structures display. This structural descriptor clearly indicates the region on the parameter space where complex micelles appear.

Given the rich phenomenology found in the case of symmetric bottlebrushes, it is expected that an asymmetry on the side chains polymerization index ($k \neq m$), could give place to a rich morphological behavior too. Thus, we explored the effect of this asymmetry on the self-assembly behavior of the mikto-grafted bottlebrushes considered in this work. For these cases, we fixed the total number of macromonomers to $n = 1000$, and the incompatibility between A and B beads to $a_{AB} = 50$. We expect that this value of the intermolecular interaction strength between A and

B polymers is large enough to allow for the presence of kinetically-trapped nanostructures if they are highly probable (for reference, a morphology map for a symmetric bottlebrush with $a_{AB} = 50$ is presented in the SI). **Figure 5** summarizes our results. For these simulations we have studied the effect of three different solvophilic side chains polymerization index, namely, $m = 10, 20$ and 50. The polymerization index of the solvophobic chains was varied from $k = 10$ to 50 as displayed on Figure 5. First, we focus on the bottlebrushes with the shorter solvophilic side chains, $m = 10$ (first row in Figure 5), which self-assembled into rod-like micelles when the type A chains are short ($k = 10$). However, by increasing the solvophobic molecular weight to $k = 20$, a toroidal structure appears as the self-assembled nanostructure (see Figure 5). By a further increase in k the nanostructures transit from ellipsoidal to spherical micelles. When the degree of polymerization of the solvophilic side chains is increased to $m = 20$ or 50 (second and third rows in Figure 5), two different kind of structures are formed. When the molecular weight of solvophobic chains is smaller than that of the solvophilic (type B) chains, bottlebrushes have a tendency to form pearl-like structures (multi-micelles). Note that these structures are equivalent to the double micelles described above for the symmetric case, and that the size of the globes are not uniform, which reinforce the notion that these are non-equilibrium structures. Finally, at larger degrees of polymerization of type A chains, spherical micelles are always formed (Figure 5).

It should be noted that the multiple-micelle structures resemble the pearl-necklace structures that have been observed in the course of the collapse of homopolymers under a fast quench to poor solvent conditions⁹²⁻⁹⁵. The scenario follows a step-wise evolution with monomers forming small clusters that stabilize, and then grow by

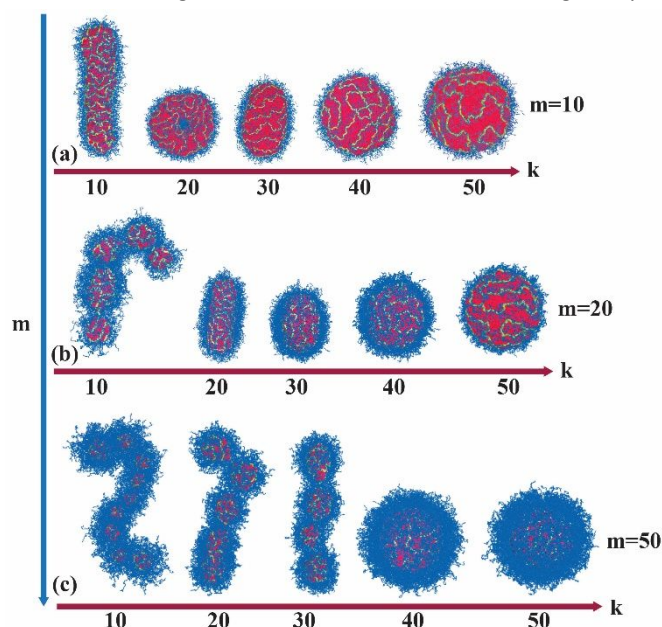


Figure 5. Representative single-polymer self-assembled nanostructures obtained after a fast quench into a bad solvent condition for one of the side chains (red domains), formed by (C-g-A_w/B_m)₁₀₀₀ asymmetric bottlebrushes. Solvophilic side chains are displayed in blue, whereas the bottlebrush backbone is represented by the green tube wrapping around the solvophobic cores. Solvent molecules are not displayed for clarity. The solvophilic block molecular weight is fixed at (a) $m=10$, (b) $m=20$, and (c) $m=50$. Solvophobic side chain molecular weight, k , increases from left to right. The chemical incompatibility between A and B polymer segments was fixed at $a_{AB} = 50$.

fusion of clusters, until all monomers form a single core. Thus, the intermediate pearl-necklace structures in homopolymers collapse are non-equilibrium structures on the way toward the equilibrium state. In our study, the solvophilic side chains help to stabilize these multi-micelle structures even more, thus, we do believe that these structures are very long-live non-equilibrium states. However, we should highlight that it has been shown that pearl-necklace structures are equilibrium states in polyelectrolyte solutions⁹⁶. Thus, to test our hypothesis about these multi-micelle structures being kinetically-trapped morphologies, we have performed additional simulations. Following Wessels and Jayaraman⁹⁷ we have applied three different protocols in which the following intermolecular parameters are varied in a gradual stage-wise increase: protocol (i), in this protocol a_{AB} is increased gradually from $a_{AB}^0=25$ to $a_{AB}^f=70$; protocol (ii), both a_{AB} and a_{AD} are increased gradually between same limits; and protocol (iii), in this case a_{AD} alone is increased gradually. In these protocols, simulations are divided into n_w stages where the parameters being varied are kept at fixed values. At every stage, simulations were run for 10^4 time steps, and the parameters were increased by $\delta a_{ij} = (a_{ij}^f - a_{ij}^0)/n_w$. For each of these protocols we used three different values of $n_w = 100, 200$ and 400. We applied these protocols to two symmetric bottlebrushes: one that forms double micelles ($n = 600, k = 20$), and another that forms triple-micelles ($n = 900, k = 20$). In all of these slow quenching protocols the final self-assembled morphology was different from the one obtained when doing a fast quench. For the short bottlebrush, which forms double micelles under a fast quench, the slow quench protocols produced either spherical or ellipsoidal micelles (a summary of these results is presented in SI). For the larger bottlebrush, which tend to form triple micelles under a fast quench, the slow quench protocols produced either toroidal or ellipsoidal micelles (see Figure 6). These results support our hypothesis that the multi-micelle morphologies are kinetically-trapped structures.

We finalize this section by highlighting two aspects of the solution self-assembly of the mikto-grafted bottlebrushes studied in this work. The first one has to do with the diversity of possible morphologies that can be obtained by exposing the macromolecules to a fast quench into a preferential solvent. The larger the number of

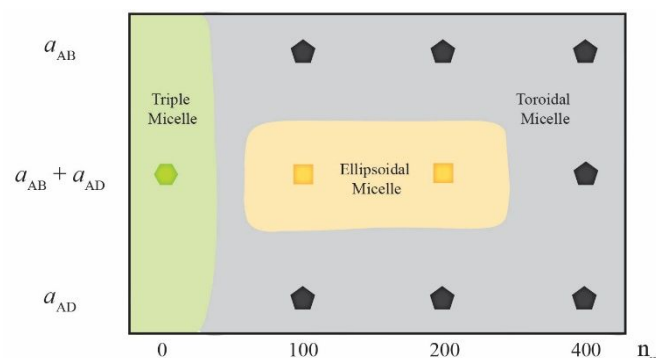


Figure 6. Self-assembled morphologies obtained by following different quenching protocols for a symmetric bottlebrush with $n = 900$ and $k = 20$. Simulations are divided into n_w stages, and at each stage the corresponding parameter(s) are increased by $\delta a_{ij} = (a_{ij}^f - a_{ij}^0)/n_w$, where $a_{ij}^0=25$ to $a_{ij}^f=70$. See text for more details. Under an instantaneous quench ($n_w = 0$) a triple-micelle structure is formed, however, by doing a slow quenching, the macromolecule self-assembled into a different morphology.

macromonomers is, the higher the probability to get kinetically-trapped nanostructures. As mentioned above, for some cases, more than one structure was obtained by starting from different initial configurations, the ones that are more frequent were presented above, but there are others that are also interesting, some of them are displayed in the SI. In the case of double and triple micelles, there are variations in the relative size of the globes forming the structures as well as in their relative spatial location. A second aspect to highlight is the stability of these kinetically-trapped structures. As mentioned in the Methods section, the simulations for bottlebrushes with a large number of macromonomers were run for more than 10^6 time steps, which is already a large number of steps considering that the model uses a soft inter-molecular interaction potential. We decided to evolve some of the final configurations for an additional 10^6 time steps, each final configuration was used to run three replicas that have different seeds for the random number generator used by DPD as implemented in HOOMD-Blue⁷⁵. Few of the configurations evolved to another morphologies, but most of them remained in their self-assembled structure, some examples are presented in the SI (Figure S9). For those morphologies that we thought have still a chance to relax even more an additional number of time steps were ran (3×10^6). These longer simulations indeed allowed some of these structures to relax. In the case of asymmetric multi-micelles, they tend to relax more easily than others, although, as expected, the relaxation time seems to be a random quantity. As can be seen double micelle structures are quite stable, for that single-realization in Fig. S9, it changed too little after 5 million-time steps. We have run another system in which a double micelle ($n = 600$) was stable for 10^7 time steps in total, and a case of a triple micelle that has been stable for 6×10^6 time steps in total. Thus, we have shown that kinetically-trapped states are common in these kinds of mikto-grafted polymer bottlebrushes under a fast quench in solvent quality. Being kinetically-trapped means that these states could still evolve towards equilibrium, however, in their evolution on the free-energy landscape they need to find the “right” path which could occur in a few time steps or millions of them. Some of these states could be metastable, and are just waiting for the proper thermal fluctuation to get out and evolve towards equilibrium. This subject itself is an exciting area that would require powerful advanced sampling techniques⁹⁸⁻¹⁰⁰ to provide some physical insights on the complicated free-energy landscape associated to these polymer systems.

Conclusions

In this work, we have performed a systematic study of the effect of several structural parameters on the solution self-assembly of molecular mikto-grafted bottlebrushes subjected to a fast change in the solvent quality of the solution. We have found the existence of a diverse set of non-equilibrium nanostructures that appear as an interplay of chemical incompatibility between solvophilic and solvophobic polymer segments, molecular weight and solvent quality. Our results emphasize that the non-equilibrium morphologies generated by the mikto-grafted bottlebrushes studied in this work can be long-lived out-of-equilibrium states and could, potentially, be realized in experiments. To avoid their eventual relaxation to equilibrium

one could use additional protocols to cross-link some of the side chains, and thus, use these complex nanostructures as templates to create organic-metallic nano-objects. In this work, we used a simple coarse-grained model that assumes that every polymer block is fully flexible, however, a more realistic simulation approach involving semiflexible chains could potentially uncover polymeric nanostructures that arise as a consequence of the bending properties of the polymer chains; work on these lines is underway and will be presented in a future report.

Conflicts of interest

There are no conflicts to declare.

Acknowledgements

A.R.-H. acknowledges the start-up support of the Faculty Science and Technology Acquisition and Retention (STARs) Program from UT System. M.H.-A. acknowledges the support of the National Science Foundation through grant CMMI-1562639. The authors are grateful to Prof. Marcus Müller and Prof. Su-Mi Hur for useful suggestions. This work received computational support from UTSA's HPC cluster SHAMU, operated by University Technology Solutions. The authors are also grateful for valuable computing resources provided by the Texas Advanced Computing Center (TACC) at The University of Texas at Austin (URL: <http://www.tacc.utexas.edu>).

Notes and references

§ Note that the degree of coarse-graining can affect the values of the intermolecular interaction parameters needed to reproduce that compressibility.

1. F. S. Bates and G. H. Fredrickson, *Physics Today*, 1999, **52**, 32-38.
2. Y. Mai and A. Eisenberg, *Chemical Society Reviews*, 2012, **41**, 5969-5985.
3. C. M. Bates and F. S. Bates, *Macromolecules*, 2017, **50**, 3-22.
4. S. Darling, *Progress in Polymer Science*, 2007, **32**, 1152-1204.
5. M. Müller, *Progress in Polymer Science*, 2020, **101**, 101198.
6. G. M. Grason, *Physics reports*, 2006, **433**, 1-64.
7. I. Hamley, *Progress in polymer science*, 2009, **34**, 1161-1210.
8. I. W. Hamley and I. W. Hamley, *The physics of block copolymers*, Oxford University Press Oxford, 1998.
9. G. Fredrickson, *The equilibrium theory of inhomogeneous polymers*, Oxford University Press on Demand, 2006.
10. F. S. Bates, M. A. Hillmyer, T. P. Lodge, C. M. Bates, K. T. Delaney and G. H. Fredrickson, *Science*, 2012, **336**, 434-440.

11. A. E. Levi, L. Fu, J. Lequieu, J. D. Horne, J. Blankenship, S. Mukherjee, T. Zhang, G. H. Fredrickson, W. R. Gutekunst and C. M. Bates, *Macromolecules*, 2020, **53**, 702-710.
12. V. Beyer, J. Kim and C. R. Becer, *Polymer Chemistry*, 2020 **11**, 1271-1291.
13. S. S. Sheiko, B. S. Sumerlin and K. Matyjaszewski, *Progress in Polymer Science*, 2008, **33**, 759-785.
14. H.-i. Lee, J. Pietrasik, S. S. Sheiko and K. Matyjaszewski, *Progress in polymer science*, 2010, **35**, 24-44.
15. J. Rzyayev, *ACS Macro Lett.* 2012, **1**, 1146-1149 .
16. R. Verduzco, X. Li, S. L. Pesek and G. E. Stein, *Chemical Society Reviews*, 2015, **44**, 2405-2420.
17. G. Xie, M. R. Martinez, M. Olszewski, S. S. Sheiko and K. Matyjaszewski, *Biomacromolecules*, 2018, **20**, 27-54.
18. H. Mei, T. S. Laws, J. P. Mahalik, J. Li, A. H. Mah, T. Terlier, P. Bonnesen, D. Uhrig, R. Kumar, G. E. Stein and R. Verduzco, *Macromolecules*, 2019, **52**, 8910-8922.
19. A. B. Chang, C. M. Bates, B. Lee, C. M. Garland, S. C. Jones, R. K. Spencer, M. W. Matsen and R. H. Grubbs, *Proceedings of the National Academy of Sciences*, 2017, **114**, 6462-6467.
20. C. M. Bates, A. B. Chang, N. a. Momčilović, S. C. Jones and R. H. Grubbs, *Macromolecules*, 2015, **48**, 4967-4973.
21. U. Tritschler, S. Pearce, J. Gwyther, G. R. Whittell and I. Manners, *Macromolecules*, 2017, **50**, 3439-3463.
22. I. Weisbord, N. Shomrat, H. Moshe, A. Sosnik and T. Segal-Peretz, *Advanced Functional Materials*, n/a, 1808932.
23. R. Fenyves, M. Schmutz, I. J. Horner, F. V. Bright and J. Rzyayev, *Journal of the American Chemical Society*, 2014, **136**, 7762-7770.
24. S. Onbulak and J. Rzyayev, *Polymer Chemistry*, 2015, **6**, 764-771.
25. S. Onbulak and J. Rzyayev, *Journal of Polymer Science Part A: Polymer Chemistry*, 2017, **55**, 3868-3874.
26. L. Xiao, L. Qu, W. Zhu, Y. Wu, Z. Liu and K. Zhang, *Macromolecules*, 2017, **50**, 6762-6770.
27. Y.-Y. Won, H. T. Davis and F. S. Bates, *Macromolecules*, 2003, **36**, 953-955.
28. S. Jain and F. S. Bates, *Macromolecules*, 2004, **37**, 1511-1523.
29. H. Cui, Z. Chen, S. Zhong, K. L. Wooley and D. J. Pochan, *Science*, 2007, **317**, 647.
30. J. L. Santos and M. Herrera-Alonso, *Macromolecules*, 2014, **47**, 137-145.
31. B. A. Aguilar-Castillo, J. L. Santos, H. Luo, Y. E. Aguirre-Chagala, T. Palacios-Hernández and M. Herrera-Alonso, *Soft Matter*, 2015, **11**, 7296-7307.
32. A. Jayaraman, D. Y. Zhang, B. L. Dewing and M. K. Mahanthappa, *ACS Central Science*, 2019, **5**, 619-628.
33. H. Luo, J. L. Santos and M. Herrera-Alonso, *Chemical Communications*, 2014, **50**, 536-538.
34. M. Müller and J. J. de Pablo, *Annual Review of Materials Research*, 2013, **43**, 1-34.
35. T. E. Gartner and A. Jayaraman, *Macromolecules*, 2019, **52**, 755-786.
36. H. P. Hsu, W. Paul and K. Binder, *Macromolecular theory and simulations*, 2007, **16**, 660-689.
37. H.-P. Hsu, W. Paul and K. Binder, *The Journal of chemical physics*, 2008, **129**, 204904.
38. H. P. Hsu, W. Paul and K. Binder, *Macromolecular theory and simulations*, 2011, **20**, 510-525.
39. A. Yethiraj, *The Journal of Chemical Physics*, 2006, **125**, 204901.
40. P. Theodorakis, W. Paul and K. Binder, *EPL (Europhysics Letters)*, 2009, **88**, 63002.
41. P. Theodorakis, W. Paul and K. Binder, *The Journal of chemical physics*, 2010, **133**, 104901.
42. H. Maleki and P. E. Theodorakis, *Journal of Physics: Condensed Matter*, 2011, **23**, 505104.
43. P. E. Theodorakis, H.-P. Hsu, W. Paul and K. Binder, *The Journal of chemical physics*, 2011, **135**, 164903.
44. P. Theodorakis, W. Paul and K. Binder, *The European Physical Journal E*, 2011, **34**, 1-12.
45. A. Chremos and P. E. Theodorakis, *ACS Macro Letters*, 2014, **3**, 1096-1100.
46. Z. Cao, W. F. Daniel, M. Vatankhah-Varnosfaderani, S. S. Sheiko and A. V. Dobrynin, *Macromolecules*, 2016, **49**, 8009-8017.
47. J. Paturej, S. S. Sheiko, S. Panyukov and M. Rubinstein, *Science Advances*, 2016, **2**, e1601478.
48. H. Liang, Z. Cao, Z. Wang, S. S. Sheiko and A. V. Dobrynin, *Macromolecules*, 2017, **50**, 3430-3437.
49. H. Liang, S. S. Sheiko and A. V. Dobrynin, *Macromolecules*, 2018, **51**, 638-645.
50. M. Jacobs, H. Liang, B. Pugnet and A. V. Dobrynin, *Langmuir*, 2018, **34**, 12974-12981.
51. S. Dutta, T. Pan and C. E. Sing, *Macromolecules*, 2019, **52**, 4858-4874.
52. M. G. Wessels and A. Jayaraman, *Soft Matter*, 2019, **15**, 3987-3998.
53. I. Lyubimov, D. J. Beltran-Villegas and A. Jayaraman, *Macromolecules*, 2017, **50**, 7419-7431.
54. I. Lyubimov, M. G. Wessels and A. Jayaraman, *Macromolecules*, 2018, **51**, 7586-7599.
55. T. Palacios-Hernandez, H. Luo, E. A. Garcia, L. A. Pacheco and M. Herrera-Alonso, *Macromolecules*, 2018, **51**, 2831-2837.
56. M. Szymusiak, J. Kalkowski, H. Luo, A. J. Donovan, P. Zhang, C. Liu, W. Shang, T. Irving, M. Herrera-Alonso and Y. Liu, *ACS Macro Letters*, 2017, **6**, 1005-1012.
57. H. Luo, D. Raciti, C. Wang and M. Herrera-Alonso, *Molecular Pharmaceutics*, 2016, **13**, 1855-1865.
58. H. Luo, M. Szymusiak, E. A. Garcia, L. L. Lock, H. Cui, Y. Liu and M. Herrera-Alonso, *Macromolecules*, 2017, **50**, 2201-2206.
59. M. Müller, *Journal of Statistical Physics*, 2011, **145**, 967-1016.
60. L.-C. Cheng, K. R. Gadelrab, K. Kawamoto, K. G. Yager, J. A. Johnson, A. Alexander-Katz and C. A. Ross, *Nano Letters*, 2018, **18**, 4360-4369.
61. K. Kawamoto, M. Zhong, K. R. Gadelrab, L.-C. Cheng, C. A. Ross, A. Alexander-Katz and J. A. Johnson, *Journal of the American Chemical Society*, 2016, **138**, 11501-11504.
62. P. Hoogerbrugge and J. Koelman, *EPL (Europhysics Letters)*, 1992, **19**, 155.
63. R. D. Groot and P. B. Warren, *The Journal of chemical physics*, 1997, **107**, 4423-4435.
64. P. Espanol and P. B. Warren, *The Journal of chemical physics*, 2017, **146**, 150901.
65. P. Espanol and P. Warren, *EPL (Europhysics Letters)*, 1995, **30**, 191.
66. V. Ortiz, S. O. Nielsen, D. E. Discher, M. L. Klein, R.

- Lipowsky and J. Shillcock, *The Journal of Physical Chemistry B*, 2005, **109**, 17708-17714.
67. L. R. Parent, E. Bakalis, A. Ramírez-Hernández, J. K. Kammeyer, C. Park, J. De Pablo, F. Zerbetto, J. P. Patterson and N. C. Gianneschi, *Journal of the American Chemical Society*, 2017, **139**, 17140-17151.
68. D. B. Wright, A. Ramírez-Hernández, M. A. Touve, A. S. Carlini, M. P. Thompson, J. P. Patterson, J. J. De Pablo and N. C. Gianneschi, *ACS Macro Letters*, 2019, **8**, 676-681.
69. J. C. Shillcock and R. Lipowsky, *Nature Materials*, 2005, **4**, 225-228.
70. A. Grafmüller, J. Shillcock and R. Lipowsky, *Physical review letters*, 2007, **98**, 218101.
71. J. C. Shillcock and R. Lipowsky, *The Journal of chemical physics*, 2002, **117**, 5048-5061.
72. R. D. Groot and T. J. Madden, *The Journal of chemical physics*, 1998, **108**, 8713-8724.
73. J. A. Anderson, C. D. Lorenz and A. Travesset, *Journal of Computational Physics*, 2008, **227**, 5342-5359.
74. J. Glaser, T. D. Nguyen, J. A. Anderson, P. Lui, F. Spiga, J. A. Millan, D. C. Morse and S. C. Glotzer, *Computer Physics Communications*, 2015, **192**, 97-107.
75. C. L. Phillips, J. A. Anderson and S. C. Glotzer, *Journal of Computational Physics*, 2011, **230**, 7191-7201.
76. W. Humphrey, A. Dalke and K. Schulten, *Journal of Molecular Graphics*, 1996, **14**, 33-38.
77. J. Aronovitz and D. Nelson, *Journal de physique*, 1986, **47**, 1445-1456.
78. D. N. Theodorou and U. W. Suter, *Macromolecules*, 1985, **18**, 1206-1214.
79. V. Blavatska and W. Janke, *The Journal of chemical physics*, 2010, **133**, 184903.
80. H. Arkin and W. Janke, *The Journal of chemical physics*, 2013, **138**, 054904.
81. A. Ramírez-Hernández, S.-M. Hur, J. C. Armas-Pérez, M. O. d. I. Cruz and J. J. De Pablo, *Polymers*, 2017, **9**, 88.
82. B. Schnurr, F. MacKintosh and D. Williams, *EPL (Europhysics Letters)*, 2000, **51**, 279.
83. B. Schnurr, F. Gittes and F. MacKintosh, *Physical Review E*, 2002, **65**, 061904.
84. H. Noguchi and K. Yoshikawa, *The Journal of Chemical Physics*, 2000, **113**, 854-862.
85. H. Noguchi and K. Yoshikawa, *The Journal of chemical physics*, 1998, **109**, 5070-5077.
86. N. V. Hud, K. H. Downing and R. Balhorn, *Proceedings of the National Academy of Sciences*, 1995, **92**, 3581-3585.
87. E. Helfand and Y. Tagami, *The Journal of Chemical Physics*, 1972, **57**, 1812-1813.
88. E. Helfand and Y. Tagami, *The Journal of Chemical Physics*, 1972, **56**, 3592-3601.
89. S.-M. Hur, V. Thapar, A. Ramírez-Hernández, G. Khaira, T. Segal-Peretz, P. A. Rincon-Delgadillo, W. Li, M. Müller, P. F. Nealey and J. J. de Pablo, *Proceedings of the National Academy of Sciences*, 2015, **112**, 14144-14149.
90. S.-M. Hur, V. Thapar, A. Ramírez-Hernández, P. F. Nealey and J. J. de Pablo, *ACS nano*, 2018, **12**, 9974-9981.
91. W. Li, P. F. Nealey, J. J. de Pablo and M. Müller, *Physical review letters*, 2014, **113**, 168301.
92. A. Halperin and P. M. Goldbart, *Physical Review E*, 2000, **61**, 565.
93. C. F. Abrams, N.-K. Lee and S. Obukhov, *EPL (Europhysics Letters)*, 2002, **59**, 391.
94. R. Chang and A. Yethiraj, *The Journal of Chemical Physics*, 2001, **114**, 7688-7699.
95. S. Majumder, J. Zierenberg and W. Janke, *Soft Matter*, 2017, **13**, 1276-1290.
96. Q. Liao, A. V. Dobrynin and M. Rubinstein, *Macromolecules*, 2006, **39**, 1920-1938.
97. M. G. Wessels and A. Jayaraman, *Soft Matter*, 2020, **16**, 623-633.
98. E. Sevgen, A. Z. Guo, H. Sidky, J. K. Whitmer and J. J. de Pablo, *Journal of Chemical Theory and Computation*, 2020, **16**, 1448-1455.
99. N. E. Jackson, M. A. Webb and J. J. de Pablo, *Current Opinion in Chemical Engineering*, 2019, **23**, 106-114.
100. A. Z. Guo, J. Lequieu and J. J. de Pablo, *The Journal of Chemical Physics*, 2019, **150**, 054902.

Table of Contents Graphic

Kinetically-Arrested Single-Polymer Nanostructures from Amphiphilic Mikto-Grafted Bottlebrushes in Solution: A Simulation Study

Bahar Gumus, Margarita Herrera-Alonso and Abelardo Ramírez-Hernández

